HetNet with Overlapping Small Cells for 5G IoT Networks[*]

YAN-JING WU[1], TSANG-LING SHEU[2,+] AND WEI-LUEN LI[2]
[1]*Department of Information Technology and Communication*
Shih Chien University
Kaohsiung Campus, Kaohsiung, 845 Taiwan
[2]*Department of Electrical Engineering*
National Sun Yat-Sen University
Kaohsiung, 804 Taiwan

Because the fifth-generation (5G) mobile wireless networks show promise in meeting the service requirements of Internet of Things, 5G systems must be equipped with the capacity to interconnect all existing and emerging technologies. To keep up with this challenge, heterogeneous networks (HetNets) can be deployed; in HetNets, the coverage area of a macro base station is embedded with many smaller base stations. This paper presents the architecture of a HetNet with overlapping small cells (HNOSC) for 5G IoT networks. The proposed HNOSC architecture considers the movement of user equipment (UE) and the overlapping area between any two small cells. We develop an analytical model by using a Markov chain of three states to derive a closed-form formula for the total downlink transmission power (TDTP) in terms of the radius of each small cell, size of the overlapping area, and UE mobility. Given the path loss factor and associated parameters of UE movement, the relationship between the coverage area of overlapping small cells and the TDTP consumption can be derived. Thus, the deployment of small base stations can be optimised to obtain the best trade-off between UE service quality and operator cost.

Keywords: macro cell, small cell, power consumption, mobility, Markov chain

1. INTRODUCTION

Advancements in mobile wireless communication technology have led to a tremendous growth in the number of wireless devices and the volume of transmitted data. One of the primary goals for the next-generation (*i.e.*, fifth-generation (5G)) mobile communication networks is to provide data rates up to 1 Gbps. This can be achieved by combining several novel communication technologies, such as massive multiple-input-multiple-output systems, millimetre-wave (mm-wave) systems, and small cell deployment [1, 2]. Research on various aspects of 5G communication, such as network architectures, communication technologies and protocols, information security, and smart applications, has been increasing. In particular, one of the main directions of development in 5G mobile networks is the implementation of systems to support Internet of Things (IoT) communications. In 2020, the number of IoT devices reached 50 billion, and the average number of devices connected to 5G communication networks was 10.3 per person (Fig. 1). In 2030, the number of IoT devices is expected to reach 80 billion, and the average number of connected devices is expected to reach 20.5 per person [1].

IoT networks with a considerably high number of device nodes require fast and low-

latency bandwidths. The deployment of heterogeneous networks (HetNets) [3, 4] is essential for meeting the requirements. A HetNet (Fig. 2) has a multitier network architecture in which a macro base station (MBS) is overlaid with small base stations (SBSs). The area covered by the MBS at the center is referred to as a macro cell (in light blue), and the area covered by an SBS is referred to as a small cell (in yellow). The antennas used in the macro/small cells can be omnidirectional or directional. However, the macro cell has considerably higher transmission power than do the small cells. User equipment (UE) located in the macro cell can access the communication system via the base stations through several approaches. If the UE is located within the range of one or more small cells, it can associate with one of them or directly associate with the macro cell in the case of bandwidth insufficiency in the small cells. However, if the UE is not located within the coverage of a small cell, then it can associate with only the macro cell. Small cells overlaid on a macro cell can provide fast, flexible, and low-cost demand-oriented transmission quality for IoT-connected devices, thereby preventing bandwidth insufficiency and network congestion in the macro cell. The existence of hot spots results in substantial performance improvements in HetNets. Furthermore, UE possesses mobility and can move between different coverage areas. For example, such equipment can move across the boundary between the macro cell and a small cell or can move between two small cells. Small cells can be subdivided into femtocells, picocells, and microcells according to their individual coverage radii in ascending order [5]. The location and number of SBSs in a HetNet affect the communication quality of IoT devices and the cost of operation and construction. However, the communication quality and the cost of operation and construction are mutually constrained. Studies [6-12] have focused on the overlaying area, number, and sleeping time of SBSs, in addition to bandwidth resource allocation for the MBS in a HetNet.
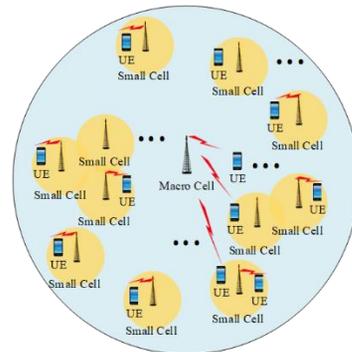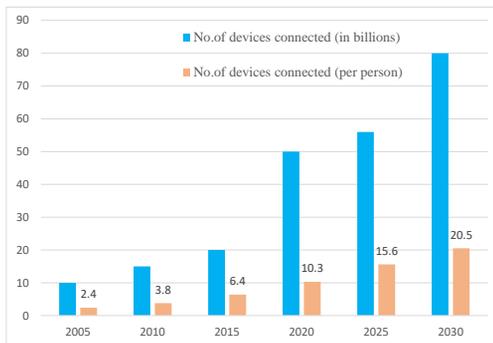
Fig. 1. Growth in the number of IoT devices (2005-2030).   Fig. 2. Typical architecture of a HetNet.

Studies [6-32] on energy consumption for the radio access network layer of a HetNet have mostly focused on the number and coverage area of SBSs, load balancing, bandwidth resource allocation, and SBS clustering. These studies can be divided into four main categories:

(1) Those analyzing the impact of clustering SBSs on the total transmission power [6, 12-15].
(2) Those focusing on allocation and spectral efficiency adjustment in SBSs and MBS to

reduce the total transmission power [7, 16-22].

(3) Those analyzing the impact of SBS sleeping time and load sharing on the system spectral efficiency and power consumption [8, 23-25].

(4) Those investigating how the number of SBSs and their individual coverage sizes affect the system spectral efficiency and power consumption [9-11, 26-32].

In summary, most of the aforementioned studies have analyzed the impact of SBS deployment, such as the number of SBSs and their location, on the system power consumption. However, they have not considered the following problems:

(1) The coverage areas of SBSs may overlap, and the size of the overlapping area (OA) strongly affects the system transmission power.

(2) UE mobility causes load variation in the MBS and SBSs, affecting the system transmission power.

To address these problems, a HetNet model with overlapping small cells (HNOSC) on a macro cell for 5G IoT networks is proposed in this paper. The proposed HNOSC model considers UE mobility as well as the size of the OA between two small cells. To obtain the optimal trade-off between UE service quality and operator cost, we establish an analytical model by using a Markov chain of three states to derive a closed-form formula for the total downlink transmission power (TDTP). Given the path loss factor and associated parameters of UE movement, the relationship between the coverage area of overlapping small cells and the total transmission power consumption can be determined.

The remainder of this paper is organized as follows. In Section 2, the proposed HNOSC is defined. In Section 3, we develop an analytical model for the HNOSC by using a Markov chain of three states to derive a closed-form formula for the TDTP. The numerical simulation results and discussion are presented in Section 4. Finally, concluding remarks are given in Section 5

2. PROPOSED HNOSC

2.1 HNOSC Architecture

Fig. 3 illustrates the proposed HNOSC architecture that supports 5G IoT network characteristics. In the proposed HNOSC model, the areas of small cells can overlap. The coverage areas in the HNOSC architecture are classified into three cell types: macro, small, and double cells. The macro cell (indicated by the large, light blue circle) represents the coverage area of the MBS and comprises many small cells. Each of the small cells (indicated by the light green circles) is composed of the range covered by an SBS. The union of two overlapping small cells is referred to as a double cell. UE is randomly distributed within the macro cell. Thus, UE can be either within the coverage of a double cell or outside. If the UE is located within the coverage of a double cell, it can be associated with either the MBS or one of the two SBSs by selecting the one with a higher signal-to-interference-plus-noise ratio. By contrast, if the UE is located outside any double cells, it can be associated only with the MBS.

Furthermore, the UE can move between different cell coverages; for example, it can move between two small cells or between the macro cell and a double cell. The proposed

HNOSC architecture considers UE mobility. UE mobility (denoted as ω) is defined as the probability of moving from one cell coverage to another during one unit of time. We assume that the moving direction of UE at a cell boundary is uniformly distributed in all angles. As displayed in the upper of Fig. 4, UE located at a cell boundary moves out of the current cell only when the movement direction is limited between $-\pi/2$ and $\pi/2$. The area of the light green ring is equivalent to that in the bottom of Fig. 4, which represents the possible area through which the UE may pass during one unit of time (denoted as t). In the bottom of Fig. 4, L and l denote the circumference and thickness, respectively, of the light green ring in the upper of Fig. 4. Let $t = 1$. Then, ω can be derived and expressed as shown in Eq. (1) according to [33, 34], where $E[V]$ and A denote the average moving speed of UE and the total area of the current cell in which the target UE is located, respectively.

$$\omega = \frac{L \times E[V]}{\pi \times A} \qquad (1)$$
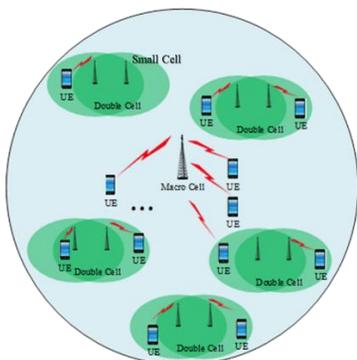
Fig. 3. HNOSC architecture.   Fig. 4. UE moving out of a cell and the equivalent area.
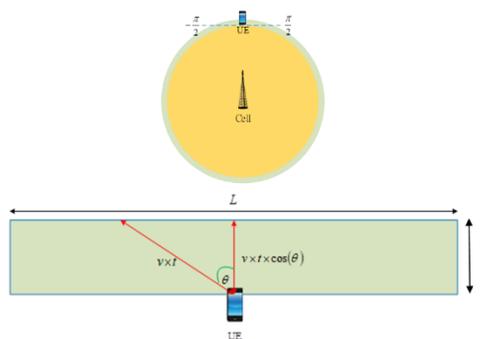
2.2 Parameters and Assumptions

To derive the TDTP in terms of the radius of each small cell, size of the OA, and UE mobility, we establish an analytical model of HNOSC by using a Markov chain of three states [35] (discussed in Section 3). The parameters used in the analytical model are listed in Table 1. N represents the total quantity of UE and m represents the total number of double cells in the system. ω represents UE mobility and $E[V]$ represents the average moving speed of the UE. R and r represent the coverage radii of the MBS and SBSs, respectively. d_c denotes the distance between the centers of two overlapping small cells for a double cell. C_s and C_r represent the total number of channels in a small cell and the minimum number of channels required for connecting UE to the system per unit of time, respectively. A channel can physically refer to a resource block, frequency band, time slot, or code. β and P_{w0} are the power attenuation factor and the reference power per unit of distance for calculating the downlink transmission power, respectively.

We can make the following assumptions for obtaining the steady-state probabilities in the analytical model:

(1) UE always moves within the coverage area of the MBS.

(2) UE can always be associated with a base station (either macro or small).
(3) UE is uniformly located within the coverage area of the MBS.

Table 1. Parameters used in the HNOSC.

Parameters	Descriptions
N	The total number of UE
m	The total number of double cells
ω	The UE mobility
$E[V]$	The average moving speed of UE
R	The coverage radius of the MBS
r	The coverage radius of an SBS
d_c	The distance between the centers of two overlapping small cells
C_s	The total number of channels in a small cell
C_r	The minimum number of channels required for a UE
β	The power attenuation factor with regard to distance
P_{W0}	The reference power per unit of distance
α	The antenna gain

3. ANALYTICAL MODEL OF HNOSC

3.1 State Transition Diagram

As illustrated in Fig. 5, the state transition diagram of the HNOSC architecture, which comprises three states, MCDC, DCMC, and DCDC, is obtained by using a Markov chain [35]. MCDC indicates that the UE is within the macro cell but not within any double cells. Thus, the UE can be associated with only the MBS in MCDC. DCMC indicates that the UE is within a certain double cell but is associated with the MBS, and DCDC indicates that the UE is within a certain double cell and is associated with one of two SBSs in the double cell. Let S_1, S_2, and S_3 be the long-run proportions of time that the Markov chain are in MCDC, DCMC, and DCDC, respectively. Alternatively, the long-run proportion of time that the Markov chain in state i is named the steady-state probability of state i. Let P_{ij} denote the transition probability from state i to state j. A total of nine transition probabilities exist in Fig. 5, which are denoted as P_{11}, P_{12}, P_{13}, P_{21}, P_{22}, P_{23}, P_{31}, P_{32}, and P_{33}. When UE is within a certain double cell and is associated with one of the two SBSs in the double cell (*i.e.* at the state DCDC), the UE hardly has an opportunity to change its association with the MBS. Consequently, P_{32} is equal to zero in Fig. 5.
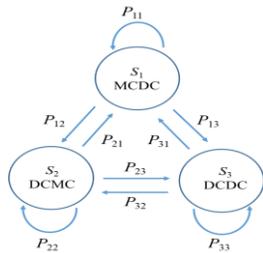
Fig. 5. State transition diagram of the HNOSC.
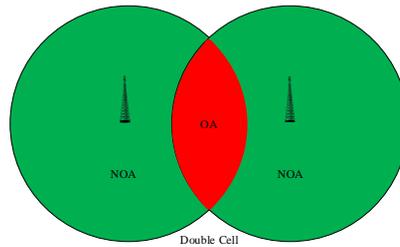
Fig. 6. Two portions of a double-cell coverage.

To derive the transition probabilities shown in Fig. 5, the UE mobility from one cell coverage to another is necessary, which is a function of the radius of a small cell (r), the distance between the centers of two SBSs for a double cell (d_c), and the average moving speed of the UE ($E[V]$). As presented in Fig. 6, the area created by each double-cell coverage overlaid on the macro cell can be divided into two regions: OA and non-OA (NOA). If the UE is within the coverage of a double cell, it can receive signals from both SBSs or only from one of the two SBSs depending on which area (OA or NOA) it is located in. As defined in Section 2.1, UE mobility is calculated using Eq. (1). In the proposed HNOSC architecture, the UE can move from one cell coverage into another through five possible cases:

(1) From the macro cell into a double cell (denoted as ω_{md})
(2) From a double cell into the macro cell (denoted as ω_{dm})
(3) From the OA into the NOA within a double cell (denoted as ω_{on})
(4) From the NOA into the OA within a double cell (denoted as ω_{no})
(5) In a double cell, but not moving out of the current double cell (denoted as ω_{dd})

The UE mobility in each of these cases can be obtained by substituting L and A in Eq. (1) with their corresponding values, which are derived as follows.

• From the macro cell into a double cell (denoted as ω_{md})

Let L_{dc} and A_{dc} denote the perimeter and coverage area of a double cell, respectively. Fig. 7 illustrates the UE mobility from the macro cell to a double cell. In this figure, L_{oa} represents the arc length of the OA; half of L_{oa} is marked in light green. Assume the existence of an isosceles triangle comprising with sides r, r, and d_c; the length of the light green arc (i.e. $L_{oa}/2$) can be formulated as shown in Eq. (2) on the basis of the theorem of cosines. L_{oa}, as indicated in Eq. (3), can be derived by rewriting Eq. (2). Then, the corresponding value of L in Eq. (1), denoted as L_{dc}, can be derived as presented in Eq. (4), and it is indicated by the bold red curve in Fig. 7. Prior to determining the corresponding value of A in Eq. (1), denoted as A_{mc}, the yellow area with slash lines in Fig. 7, denoted as A_s, is derived as Eq. (5) by subtracting the sector with radius r and angle φ from the area of the aforementioned isosceles triangle. Then, the size of the OA (denoted as A_{oa}) is the difference between the area of the regular rhombus and $4A_s$, as expressed in Eq. (6). The coverage area of a double cell (i.e. A_{dc}) is obtained by subtracting A_{oa} from $2\pi r^2$, as expressed in Eq. (7). Therefore, A_{mc}, which represents the coverage area of the macro cell excluding A_{dc}, can be derived using Eq. (8). Finally, as presented in Eq. (9), ω_{md} is obtained by replacing L and A in Eq. (1) with L_{dc} and A_{mc}, respectively.

$$L_{oa}\Big/2 = r \times \phi = r \times \cos^{-1}\left(\frac{r^2 + d_c^2 - r^2}{2 \times r \times d_c}\right) \tag{2}$$

$$L_{oa} = 2 \times r \times \cos^{-1}\left(\frac{d_c}{2r}\right) \tag{3}$$

$$L_{dc} = 4\pi r - 4 \times r \times \cos^{-1}\left(\frac{d_c}{2r}\right) \tag{4}$$

$$A_s = \frac{d_c \times r}{2} \times \sqrt{1 - \left(\frac{d_c}{2r}\right)^2} - r^2 \times \cos^{-1}\left(\frac{d_c}{2r}\right) \tag{5}$$

$$A_{oa} = 4 \times r^2 \cos^{-1}\left(\frac{d_c}{2r}\right) - d_c \times r \times \sqrt{1 - \left(\frac{d_c}{2r}\right)^2} \tag{6}$$

$$A_{dc} = 2\pi r^2 - \left[4 \times r^2 \times \cos^{-1}\left(\frac{d_c}{2r}\right) - d_{dc} \times r \times \sqrt{1 - \left(\frac{d_c}{2r}\right)^2}\right] \tag{7}$$

$$A_{mc} = \pi R^2 - \left\{2\pi r^2 - \left[4 \times r^2 \times \cos^{-1}\left(\frac{d_c}{2r}\right) - d_{dc} \times r \times \sqrt{1 - \left(\frac{d_c}{2r}\right)^2}\right]\right\} \tag{8}$$

$$\omega_{md} = \frac{E[V] \times L_{dc}}{\pi \times A_{mc}} \tag{9}$$

- From a double cell into the macro cell (denoted as ω_{dm})

Fig. 8 illustrates the UE mobility from a double cell into the macro cell. By substituting L and A in Eq. (1) with its corresponding values L_{dc} and A_{dc}, respectively, we can derive ω_{dm} as shown in Eq. (10), where L_{dc} and A_{dc} are derived in the preceding case.

$$\omega_{dm} = \frac{E[V] \times L_{dc}}{\pi \times A_{dc}} \tag{10}$$
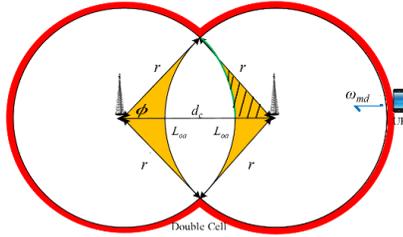
Fig. 7. Illustration of ω_{md}.   Fig. 8. Illustration of ω_{dm}.
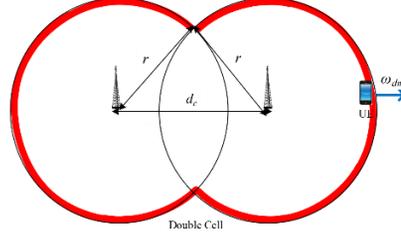
- From the OA into NOA within a double cell (denoted as ω_{on})

Fig. 9 illustrates the UE mobility from the OA into the NOA within a double cell. The perimeter of the OA region is $2L_{oa}$, where L_{oa} is calculated using Eq. (3). The area of the OA region (*i.e.* A_{oa}) is calculated using Eq. (6). Therefore, ω_{on} can be obtained by substituting L and A in Eq. (1) with $2L_{oa}$ and A_{oa}, respectively, as expressed in Eq. (11).

$$\omega_{on} = \frac{E[V] \times 2L_{oa}}{\pi \times A_{oa}} \tag{11}$$

- From the NOA into the OA within a double cell (denoted as ω_{no})

Fig. 10 displays the UE mobility from the NOA into the OA within a double cell. Here, the corresponding value of L in Eq. (1) is equal to $2L_{oa}$, and the corresponding value of A in Eq. (1) is derived by subtracting A_{oa} from A_{dc}, where A_{dc} and A_{oa} are already derived as Eqs. (7) and (6), respectively. Then, ω_{no} can be formulated as Eq. (12).

$$\omega_{no} = \frac{E[V] \times 2L_{oa}}{\pi \times (A_{dc} - A_{oa})} \tag{12}$$
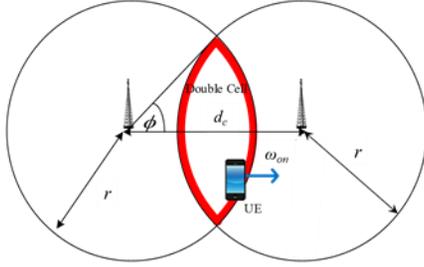
Fig. 9. Illustration of ω_{on}.
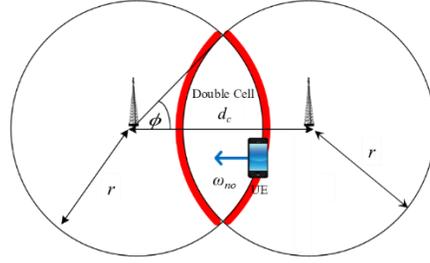
Fig. 10. Illustration of ω_{no}.

• In a double cell, but not moving out of the current double cell (denoted as ω_{dd})
Because ω_{dm} indicates the UE mobility from a double cell into the macro cell, ω_{dd} can be derived as follows:

$$\omega_{dd} = 1 - \frac{E[V] \times L_{dc}}{\pi \times A_{dc}}. \tag{13}$$

Then, the nine transition probabilities can be formulated using Eqs. (14)-(22), where μ_{oa} and μ_{na} denote the probabilities of the UE being located within the OA and NOA regions, respectively, in the event that they have no available channels to allocate.

$$P_{12} = \omega_{md} \times \mu_{na} \tag{14}$$

$$P_{13} = \omega_{md} \times (1 - \mu_{na}) \tag{15}$$

$$P_{11} = 1 - (P_{12} + P_{13}) \tag{16}$$

$$P_{21} = \omega_{dm} \tag{17}$$

$$P_{23} = \omega_{on} \times (1 - \mu_{na}) + \omega_{no} \times (1 - \mu_{oa}) \tag{18}$$

$$P_{22} = 1 - (P_{21} + P_{23}) \tag{19}$$

$$P_{31} = \omega_{dm} \tag{20}$$

$$P_{32} = 0 \tag{21}$$

$$P_{33} = 1 - P_{31} \tag{22}$$

As described in Section 2.2, we assume that all pieces of UE are uniformly located within the coverage area of the MBS and denote the total number of channels for an SBS as C_s. Let C_{oa} and C_{noa} denote the total available channels for the OA and NOA regions of a double cell, respectively; they can be obtained using Eqs. (23) and (24), respectively. Before deriving the probability of the UE being located within the OA region that has no available channels to allocate (*i.e.* μ_{oa}), we must determine the possible quantity of UE located within the OA region, which is denoted as N_1 and obtained using Eq. (25). N_1 comprises three terms, N_{oa}, N_{no}, and N_{on}, which denote the quantity of UE initially located within the OA region, the average quantity of UE moving from the NOA into OA regions, and the average quantity of UE moving from the OA into NOA regions, respectively. The three terms on the right-hand side of Eq. (25) can be formulated as Eqs. (26)-(28). UE

within the OA region of a double cell would receive service if the product of N_1 and C_r is greater than C_{oa}, where C_r denotes the minimum number of channels required for UE, as defined in Section 2.2. Otherwise, it would not receive service. Accordingly, μ_{oa} can be formulated as Eq. (29).

$$C_{oa} = 2 \times C_s \times \frac{A_{oa}}{\pi r^2} \tag{23}$$

$$C_{noa} = 2 \times C_s \times \left(1 - \frac{A_{oa}}{\pi r^2}\right) \tag{24}$$

$$N_1 = N_{oa} + N_{no} - N_{on} \tag{25}$$

$$N_{oa} = N \times \frac{A_{oa}}{\pi R^2} \tag{26}$$

$$N_{no} = N \times \frac{A_{dc} - A_{oa}}{\pi R^2} \times \omega_{no} \tag{27}$$

$$N_{on} = N \times \frac{A_{oa}}{\pi R^2} \times \omega_{on} \tag{28}$$

$$\mu_{oa} = \begin{cases} 1 - \dfrac{C_{oa}}{C_r N_1}, & C_r N_1 > C_{oa} \\ 0, & else \end{cases} \tag{29}$$

Similarly, before we determine the probability of the UE being located within the NOA region that has no available channels for allocation (*i.e.* μ_{na}), we can derive the possible quantity of UE located within the NOA region, denoted as N_2, as expressed in Eq. (30). N_2 comprises five terms: N_{noa}, N_{md}, N_{on}, N_{dm}, and N_{no}. N_{on} and N_{no} are already defined and formulated previously; N_{noa} denotes the quantity of UE initially located within the NOA region, N_{md} denotes the average quantity of UE moving from the macro cell into a double cell, and N_{dm} denotes the average quantity of UE moving from a double cell into the macro cell. N_{noa}, N_{md}, and N_{dm} can be formulated as Eqs. (31)-(33). UE located within the NOA region of a double cell receives service if the product of N_2 and C_r is greater than C_{noa}. Otherwise, it would not receive service. Similar to Eq. (29), μ_{na} can be formulated as Eq. (34).

$$N_2 = N_{noa} + N_{md} + N_{on} - N_{dm} - N_{no} \tag{30}$$

$$N_{noa} = N \times \frac{A_{dc} - A_{oa}}{\pi R^2} \tag{31}$$

$$N_{md} = N \times \left(1 - \frac{A_{dc}}{\pi R^2}\right) \times \omega_{md} \tag{32}$$

$$N_{dm} = N \times \frac{A_{dc} - A_{oa}}{\pi R^2} \times \omega_{dm} \tag{33}$$

$$\mu_{na} = \begin{cases} 1 - \dfrac{C_{noa}}{C_r N_2}, & C_r N_2 > C_{noa} \\ 0, & else \end{cases} \tag{34}$$

Finally, the three steady-state probabilities, S_1, S_2, and S_3, can be obtained by solving the following system of linear equations.

$$\begin{cases} P_{11}S_1 + P_{21}S_2 + P_{31}S_3 = S_1 \\ P_{12}S_1 + P_{22}S_2 + P_{32}S_3 = S_2 \\ P_{13}S_1 + P_{23}S_2 + P_{33}S_3 = S_3 \\ S_1 + S_2 + S_3 = 1 \end{cases} \tag{35}$$

3.2 TDTP Derivation

To determine the TDTP for the proposed HNOSC architecture, let Pw_1, Pw_2, and Pw_3 be the downlink transmission power of UE in MCDC, DCMC, and DCDC, respectively. Pw_1, Pw_2, and Pw_3 pertain to the coverage radius of the base station, the reference power per unit distance (*i.e.* Pw_0), and the power distance attenuation coefficient (*i.e.* β). Using β and Pw_0 defined in Section 2.2, we can express Pw_1, Pw_2, and Pw_3 as Eqs. (36)-(38), where α stands for the antenna gain. Thus, the TDTP for the macro cell and each double cell, denoted as Pm and Pd, respectively, can be obtained using Eqs. (39) and (40), respectively. As shown in Eq. (41), the TDTP consumed in the system, denoted as Pt, is obtained by summing Pm and Pd. Thus, the TDTP consumed in the system can be represented by a closed-form formula in terms of the coverage radii for the MBS and SBSs, size of the OA, and UE mobility. The deployment of SBSs can be optimised to obtain the best trade-off between UE service quality and operator cost.

$$Pw_1 = \left(\frac{R}{\alpha}\right)^{\beta} Pw_0 \tag{36}$$

$$Pw_2 = \left(\frac{R}{\alpha}\right)^{\beta} Pw_0 \tag{37}$$

$$Pw_3 = \left(\frac{r}{\alpha}\right)^{\beta} Pw_0 \tag{38}$$

$$Pm = N\left(Pw_1 S_1 + Pw_2 S_2\right) \tag{39}$$

$$Pd = NPw_3 S_3 \tag{40}$$

$$Pt = N\left(Pw_1 S_1 + Pw_2 S_2 + Pw_3 S_3\right) \tag{41}$$

4. NUMERICAL SIMULATIONS

4.1 Parameters and Values

We present an evaluation of the system performance of the proposed HNOSC architecture by using the analytical model developed in Section 3. The parameter settings are presented in Table 2. The total number of UE or IoT devices, denoted as N, is set to 1000. The transmission radii of the MBS and each SBS (*i.e.* R and r) are maintained at 5000 and 150 meters, respectively. Because the size of the OA region of a double cell is related to r, we assume that the distance between the centers of two overlapping small cells is $0.2r$.

Table 2. Parameters and settings.

Parameters	Settings
The total number of UE (N)	1000
The coverage radius of the MBS (R)	5000 meters
The coverage radius of an SBS (r)	150 meters
The distance between the centers of two small cells (d_c)	30 meters
The total number of channels in a small cell (C_s)	10
The min. number of channels required for a UE (C_r)	1
The power attenuation factor with regard to distance (β)	2
The reference power per unit of meter (Pw_0)	1 nano-Watt
The antenna gain (α)	2
The total number of double cells (m)	3~29
The average moving speed of UE ($E[V]$)	2~20 meters/second

Accordingly, the diameter of a double cell is 330 meters. The total number of channels in a small cell (*i.e.* C_s) is 10, and the minimum number of channels required for a piece of UE (*i.e.* C_r) is 1. The reference power per meter is 1 nano-Watt. The power attenuation factor with regard to distance is set to 2. The antenna gain is fixed at 2. By varying the total number of double cells (*i.e.* m) within the macro cell and the average moving speed of UE (*i.e.* $E[V]$), we observe the impact of these parameters on the TDTP. The corresponding transition probabilities between any two states in the analytical model for the proposed HNOSC can be derived. The steady-state probabilities for the three states and the TDTP consumed in the system are obtained by running the calculations on MATLAB [36].

4.2 Results and Discussions

The average moving speed of UE is set to 10 meters/s and Fig. 11 shows the TDTP for different numbers of double cells (*i.e.* m). As illustrated in this figure, the blue curve (*i.e.* Pm, as expressed by Eq. (39)) exhibits a declining trend, whereas the red curve (*i.e.* Pd, as expressed by Eq. (40)) increases with m. This is because the higher the number of double cells is, the larger the coverage area of double cells is in the HNOSC architecture, which in turn leads to the decrease in the quantity of UE connected to the macro cell; that is, Pm decreases as m increases. This also explains why Pd increases with m. The two curves, Pm and Pd, intersect when m is approximately 25. This is because the probability of UE connecting to the macro cell is much lower than that of UE connecting to a double cell at $m = 25$ and because Pm and Pd are positively related to their individual coverage radii (*i.e.* R and r). R is much larger than r. Therefore, the increase in the coverage area of double cells gradually enhances the TDTP consumed in all double cells, and finally, Pd exceeds Pm at the crossover point. According to Eq. (41), the curve in grey shows the TDTP consumed in the system (*i.e.* Pt). Pt decreases as m increases until m is 23 but exhibits an upward trend when m exceeds 23. Regarding the concave curve, the minimum Pt at m is approximately 23.

Furthermore, we set the number of double cells to 21 and 25, respectively. The average moving speed of UE (*i.e.* $E[V]$) is changed from 2 to 20 meters/s with a 2 meters/s increment. Fig. 12 shows the TDTP variation with respect to different average moving speeds; Pd increases but Pm decreases with the increase in $E[V]$, regardless of N. The probability of UE moving from the macro cell into a double cell (*i.e.* ω_{md}) is higher than

that of UE moving from a double cell into the macro cell (*i.e.* ω_{dm}) because the coverage area of all double cells is always larger than the macro cell coverage at both *m* values. That is, the quantity of UE moving into double cells is greater than that of UE moving out of double cells; thus, more UE is disconnected from the MBS and connects to the SBSs. This phenomenon becomes more obvious with the increase in $E[V]$. This thus explains why *Pd* increases but *Pm* decreases when $E[V]$ is increased. Moreover, *Pm* derived at $m = 21$ (*i.e.* the blue curve with circle marks) is higher than that derived at $m = 25$ (*i.e.* the blue curve with diamond marks) because that derived at $m = 21$ has a smaller coverage area of double cells. In contrast to *Pm*, *Pd* derived at $m = 21$ (*i.e.* the red curve with circle marks) is lower than that derived at $m = 25$ (*i.e.* the red curve with diamond marks) due to the same reason.
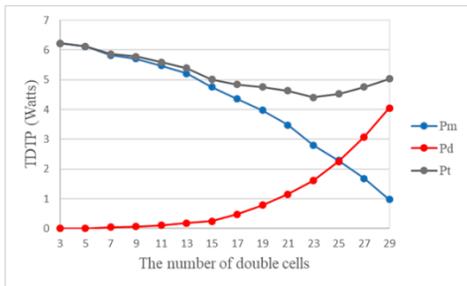
Fig. 11. *Pm*, *Pd*, and *Pt* versus *m*.   Fig. 12. *Pm* and *Pd* versus $E[V]$.
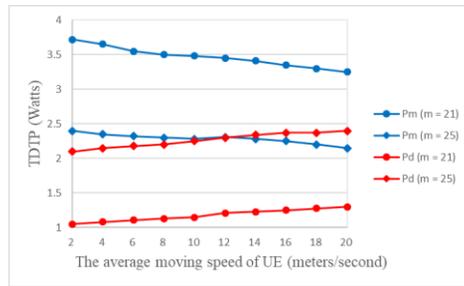
5. CONCLUSIONS

This paper proposes a HetNet with overlapping small cells (HNOSC) for 5G IoT networks. The proposed HNOSC considers not only the overlapping coverage between two small cells but also the UE mobility. To obtain the best trade-off between UE service quality and operator cost by optimising the deployment of SBSs, we develop a state transition diagram that includes three states, MCDC, DCMC, and DCDC, with nine transition probabilities between any two states based on the theory of Markov chains. The steady-state probabilities of MCDC, DCMC, and DCDC are obtained by solving a system of linear equations derived from the state transition diagram. Subsequently, the TDTP consumed in the system is determined. Numerical simulation results reveal that setting an appropriate area covered by all small cells results in the minimum TDTP when the coverage radii of the MBS and SBSs, size of the OA between any two small cells, and average moving speed of UE are given. In future studies, we will investigate a HetNet with three or more overlapping small cells and with different movement models of UE in the macro cell.

REFERENCES

1. L. Chettri and R. Bera, "A comprehensive survey on Internet of Things (IoT) toward 5G wireless systems," *IEEE Internet of Things Journal*, Vol. 7, 2020, pp. 16-32.
2. M. R. Palattella *et al.*, "Internet of Things (IoT) in the 5G era: Enablers, architecture, and business models," *IEEE Journal of Selected Areas in Communications*, Vol. 34, 2016, pp. 510-527.

3. H. Elsawy, E. Hossain, and D. I. Kim, "HetNets with cognitive small cells: User offloading and distributed channel access techniques," *IEEE Communications Magazine*, Vol. 51, 2013, pp. 28-36.

4. C. Khirallah and J. Thompson, "Energy efficiency of heterogeneous networks in LTE-advanced," *Journal of Signal Processing Systems*, Vol. 69, 2012, pp. 105-113.

5. A. Radwan, M. F. Domingues, and J. Rodriguez, "Mobile caching-enabled small-cells for delay-tolerant e-health apps," in *Proceedings of IEEE International Conference on Communications*, 2017, pp. 103-108.

6. W. Dghais, M. Souilem, Hao R. Chi, A. Radwan, and Abd-Elhamid M. Taha, "Dynamic clustering for power effective small cell deployment in HetNet 5G networks," in *Proceedings of IEEE International Conference on Communications*, 2020, pp. 1-5.

7. J.-S. Liu, C.-H. R. Lin, and Y.-C. Hu, "Joint resource allocation, user association, and power control for 5G LTE-based heterogeneous networks," *IEEE Access*, Vol. 8, 2020, pp. 122654-122672.

8. Q. Zhang, X. Xu, J. Zhang, X. Tao, and C. Liu, "Dynamic load adjustments for small cells in heterogeneous ultra-dense networks," in *Proceedings of IEEE Wireless Communications and Networking Conference*, 2020, pp. 1-6.

9. A. M. Alqasir and A. E. Kamal, "Cooperative small cell HetNets with dynamic sleeping and energy harvesting," *IEEE Transactions on Green Communications and Networking*, Vol. 4, 2020, pp. 774-782.

10. A. Dataesatu, P. Boonsrimuang, K. Mori, and P. Boonsrimuang, "Energy efficiency enhancement in 5G heterogeneous cellular networks using system throughput based sleep control scheme," in *Proceedings of the 22nd International Conference on Advanced Communication Technology*, 2020, pp. 549-553.

11. G. Ghatak, A. De Domenico, and M. Coupechoux, "Small cell deployment along roads: Coverage analysis and slice-aware RAT selection," *IEEE Transactions on Communications*, Vol. 67, 2019, pp. 5875-5891.

12. D. Ghozlani, S. Bouallegue, A. Omri, A. Busson, and R. Bouallegue, "Enhancing energy efficiency by neighbors-aware algorithm in femtocell networks," in *Proceedings of the 15th International Wireless Communications and Mobile Computing Conference*, 2019, pp. 1323-1327.

13. Y. L. Chung, "Energy-saving transmission for green Macrocell-small cell systems: A system-level perspective," *IEEE Systems Journal*, Vol. 22, 2015, pp. 706-716.

14. K. Y. Lin, J. Y. Chen, F. C. Ren, and C. J. Chang, "TAPS: Traffic-aware power saving scheme for clustered small cell base stations in LTE-A," in *Proceedings of IEEE 81st Vehicular Technology Conference*, 2015, pp. 1-5.

15. Y. Zhao, H. Xia, and Z. Zeng, "Grouping based power control for improving energy efficiency in dense small cell networks," in *Proceedings of IEEE 26th Annual International Symposium on Personal*, *Indoor*, *and Mobile Radio Communications*, 2015, pp. 1644-1648.

16. M. Yousefvand, T. Han, N. Ansari, and A. Khreishah, "Distributed energy-spectrum trading in green cognitive radio cellular networks," *IEEE Transactions on Green Communications and Networking*, Vol. 1, 2017, pp. 253-263.

17. X. Zhang, J. Zhang, and W. Wang, "Macro-assisted data-only carrier for 5G green cellular systems," *IEEE Communications Magazine*, Vol. 53, 2015, pp. 223-231.

18. M. Ismail, K. Qaraqe, and E. Serpedin, "Cooperation incentives and downlink radio

resource allocation for green communications in a heterogeneous wireless environment," *IEEE Transactions on Vehicular Technology*, Vol. 65, 2015, pp. 1627-1638.

19. A. Prasad, A. Maeder, and C. Ng, "Energy efficient small cell activation mechanism for heterogeneous networks," in *Proceedings of IEEE Globecom Workshops*, 2013, pp. 754-759.

20. H. C. Jang and P. Y. Huang, "Adaptive energy saving strategy for LTE-advanced networks," in *Proceedings of the 7th International Conference on Ubiquitous and Future Networks*, 2015, pp. 306-310.

21. G. He, S. Zhang, Y. Chen, and S. Xu, "Architecture design and performance evaluation for future green small cell wireless networks," in *Proceedings of IEEE International Conference on Communications Workshops*, 2013, pp. 1178-1182.

22. Y. Jin, L. Qiu, and X. Liang, "Small cells on/off control and load balancing for green dense heterogeneous networks," in *Proceedings of IEEE Wireless Communications and Networking Conference*, 2015, pp. 1530-1535.

23. C. Yang, J. Yue, M. Sheng, and J. Li, "Trade-off between energy-efficiency and spectral-efficiency by cooperative rate splitting," *Journal of Communications and Networks*, Vol. 16, 2014, pp. 121-129.

24. H. Holtkamp, G. Auer, S. Bazzi, and H. Haas, "Minimizing base station power consumption," *IEEE Journal of Selected Areas in Communications*, Vol. 32, 2014, pp. 297-306.

25. C. H. Liu and L. C. Wang, "Optimal cell load and throughput in green small cell networks with generalized cell association," *IEEE Journal of Selected Areas in Communications*, Vol. 34, 2016, pp. 1058-1072.

26. P. Masek, M. Slabicki. J. Hosek, and K. Grochla, "Transmission power optimization in live 3GPP LTE-A indoor deployment," in *Proceedings of the 8th International Congress on Ultra-Modern Telecommunications and Control Systems and Workshops*, 2016, pp. 164-170.

27. Y. L. Chung, "An efficient coverage algorithm for use in Macrocell-small cell systems," in *Proceedings of IEEE International Systems Engineering Symposium*, 2017, pp. 1-5.

28. M. M. Mowla, I. Ahmad, D. Habibi, and Q. V. Phung, "A green communication model for 5G systems," *IEEE Transactions on Green Communications and Networking*, Vol. 1, 2017, pp. 264-280.

29. S. Cai, L. Duan, J. Wang, and R. Zhang, "Power-saving heterogeneous networks through optimal small-cell scheduling," in *Proceedings of IEEE Global Conference on Signal and Information Processing*, 2014, pp. 188-192.

30. Y. L. Chung, "An energy-saving small-cell zooming scheme for two-tier hybrid cellular networks," in *Proceedings of IEEE International Conference on Information Networking*, 2015, pp. 148-152.

31. A. Arbi and T. O' Farrell, "Energy efficiency in 5G access networks: Small cell densification and high order sectorization," in *Proceedings of IEEE International Conference on Communication Workshop*, 2015, pp. 2806-2811.

32. X. Ge, T. Han, Y. Zhang, G. Mao, C. X. Wang, J. Zhang, B. Yang, and S. Pan, "Spectrum and energy efficiency evaluation of two-tier femtocell networks with partially open channels," *IEEE Transactions on Vehicular Technology*, Vol. 63, 2013, pp. 1306-1319.

33. H. Xie and S. Kuek, "Priority handoff analysis," in *Proceedings of the 43rd IEEE Vehicular Technology Conference*, 1993, pp. 855-858.
34. H. Xie and D. J. Goodman, "Mobility models and biased sampling problem," in *Proceedings of the 2nd International Conference on Universal Personal Communications Personal Communications*, Vol. 2, 1993, pp. 803-807.
35. S. M. Ross, *Introduction to Probability Models*, 11th ed., Academic Press, USA, 2014.
36. MATLAB, https://www.mathworks.com/products/matlab.html

Yan-Jing Wu (吳妍靚) received the Ph.D. degree in Computer Engineering from the Department of Electrical Engineering, National Sun Yat-Sen University, Kaohsiung, Taiwan. She became an Assistant Professor in 2007, and was promoted to Associate Professor in 2013 at the Department of Information Technology and Communication, Shih Chien University, Kaohsiung Campus, Taiwan. Her research interests are in the area of mobile wireless communication networks and the state-of-the-art networking systems, with emphasis on resource allocation and mobility management for multimedia traffic.

Tsang-Ling Sheu (許蒼嶺) received the Ph.D. degree in Computer Engineering from the Department of Electrical and Computer Engineering, Penn State University, University Park, Pennsylvania, USA, in 1989. From September 1989 to July 1995, he worked with IBM Corporation at Research Triangle Park, North Carolina, USA. In Aug. 1995, he became an Associate Professor, and was promoted to Professor in January 2006 at the Department of Electrical Engineering, National Sun Yat-Sen University, Kaohsiung, Taiwan. His research interests include mobile wireless networks and multimedia networking.

Wei-Luen Li (李偉綸) received the MS degree from the Department of Electrical Engineering, National Sun Yat-Sen University, Kaohsiung, Taiwan, in February 2018. Currently, he is a system programmer for a system integration company located in Shin-Chu Scientific Park, Taiwan. His research interests include applying queuing theory for analyzing wireless and mobile communication networks, such as 4G/5G sectoral networks.